ChemPubSoc Europe

DOI: 10.1002/cssc.201200907

Synthesis of DNL-6 with a High Concentration of Si(4Al) Environments and its Application in CO_2 Separation

Xiong Su,[a, b] Peng Tian,[a] Dong Fan,[a, b] Qinghua Xia,[c] Yue Yang,[a] Shutao Xu,[a] Lin Zhang,[a] Ying Zhang,[a] Dehua Wang,[a, b] and Zhongmin Liu*[a]

The synthesis of DNL-6 with a high concentration of Si(4Al) environments [Si/(Si+Al+P) = 0.182 mol, denoted as M-DNL-6] is demonstrated. This represents the highest reported concentration of such environments in silicoaluminophosphate (SAPO) molecular sieves. Adsorption studies show that the high Si(4Al) content in M-DNL-6, with an increased number of Brønsted acid sites in the framework, greatly promotes the adsorption of CO_2. M-DNL-6 exhibits a large CO_2 uptake capacity of up to 6.18 mmol g^{-1} at 273 K and 101 kPa, and demonstrates high ratios of CO_2/CH_4 and CO_2/N_2 separation. From breakthrough and cycling experiments, M-DNL-6 demonstrates the ability to completely separate CO_2 from CH_4 or N_2 with a dynamic capacity of approximately 8.0 wt% before breakthrough. Importantly, the adsorbed CO_2 is easily released from the adsorbent through a simple gas purging operation at room temperature to regain 95% of the original adsorption capacity. These results suggest that M-DNL-6 can be used as a potential adsorbent for CO_2 capture in pressure swing adsorption processes.

Introduction

Microporous crystalline materials that possess intrinsic aperture sizes of molecular dimensions have shown potential for applications in gas separations and catalysis.[1–6] Among these processes, selective CO_2 adsorption from gaseous mixtures is of paramount importance, which attracts attention because of global warming.[7,8] In addition, the separation of CO_2 from CH_4 is also an issue in natural-gas processing. The existence of CO_2 reduces the energy content of natural gas and causes pipeline corrosion.[9] At present, the industrial technology that is used for the removal of CO_2 from gas streams is based on absorption in aqueous solutions of amines; however, this method is highly complex and results in corrosion of the equipment.[10] Therefore, it is important to develop energy-efficient and economic alternatives that can achieve effective separation under ambient conditions.

Much attention has been paid to the development of adsorption methods that utilize nanoporous materials as adsorbents, such as pressure swing adsorption (PSA). The main advantages of the PSA process for gas separation are lower energy consumption and that chemical solvents are not required. According to published literature reports, a number of micro- and mesoporous materials have been used for CO_2/CH_4 separation, such as zeolites,[11–14] active carbon materials,[15] metal–organic frameworks (MOFs),[16,17] zeolitic-imidazolate frameworks (ZIFs),[7] and functionalized mesoporous silica.[18] Promising candidates for such PSA processes should have a high capacity for the selective adsorption of CO_2 with facile recycling.

In principle, porous materials that have pore sizes between the kinetic diameters of CO_2 (3.30 Å) and CH_4 (3.82 Å) or CO_2 and N_2 (3.64 Å),[19] and have adequate Coulomb potentials with gas molecules,[20] should have a superior separation efficiency. Numerous small-pore molecular sieves with eight ring-openings have been examined as CO_2 adsorbents.[21–23] Palomino et al. investigated zeolites with Linde Type A (LTA) structures containing different Si/Al ratios as adsorbents for CO_2/CH_4 separation. LTA zeolites have offered unique possibilities for CH_4 to upgrade from natural gas, and the Al content had a positive effect on the CO_2/CH_4 selectivity and the regeneration ability of the samples.[13] Palomino et al.[24] and Liu et al.[25] reported effective CO_2/CH_4 and CO_2/N_2 separations by using small-pore RHO zeolites and AlPO-type molecular sieves, respectively, which had suitable pore diameters. In addition, an ideal selectivity of CO_2/N_2 was also obtained by tuning the pore size of

[a] X. Su, Dr. P. Tian, D. Fan, Y. Yang, Dr. S. Xu, Dr. L. Zhang, Dr. Y. Zhang, D. Wang, Prof. Z. Liu
Dalian National Laboratory for Clean Energy
Dalian Institute of Chemical Physics
Chinese Academy of Sciences
457 Zhongshan Road, Dalian 116023 (PR China)
Fax: (+86) 411-84379289
E-mail: liuzm@dicp.ac.cn

[b] X. Su, D. Fan, D. Wang
Graduate University of Chinese Academy of Sciences
Beijing, 100039 (PR China)

[c] Prof. Q. Xia
Ministry-of-Education Key Laboratory for the Synthesis and Application of Organic Functional Molecules
School of Chemistry and Chemical Engineering
Hubei University
Wuhan, 430062 (PR China)

Supporting Information for this article is available on the WWW under http://dx.doi.org/10.1002/cssc.201200907.

a NaKA zeolite with an optimal K^+ content of 9.9 atom%.[26] Also, a series of univalent cation-exchanged RHO zeolites have been examined in detail as CO_2 adsorbents, which demonstrated remarkable CO_2 adsorption that resulted from a combination of the flexible framework structure, the distribution of extra-framework cations over different sites, and the mobility of the cations occupying window sites between the α-cages.[27]

DNL-6 is an isomorphous crystal of the RHO zeolite with a SAPO-based composition, which was recently reported by our group. DNL-6 possesses a large pore volume (0.36 $cm^3 g^{-1}$) and good thermal stability up to 1373 K;[28–30] however, the Si content in DNL-6 is restricted to a narrow concentration range, and varying the Si content in the starting gel can lead to the emergence of SAPO-34. DNL-6 exhibits a suitable pore size (3.6 Å) and is, therefore, a potential candidate for the selective adsorption of CO_2; this was verified in our preliminary work.[31] Recently, Hedin et al. studied the CO_2 adsorption properties of several SAPO-based molecular sieves, including DNL-6. A CO_2 capacity of 3.61 mmol g^{-1} on DNL-6 was obtained at 273 K and 101 kPa.[21] They also determined that SAPO-based molecular sieves are less moisture-sensitive than zeolite 13X, which is an important characteristic in the application of an adsorbent.

Herein, we report a method to synthesize DNL-6 with a high concentration of Si(4Al) environments. Three DNL-6 samples containing different silicon contents were used as adsorbents for the separations of CO_2 from CH_4 and N_2, and excellent results were obtained. The influence of the Si content on the adsorption properties of DNL-6 was investigated, which was demonstrated to be important. Breakthrough experiments were performed to determine the dynamic adsorption selectivity and regeneration ability of the adsorbents. Moreover, commercial zeolites NaA and SAPO-34 were also used as reference adsorbents.

Results and Discussion

Synthesis and characterization of DNL-6

M-DNL-6 was synthesized by using SAPO dry gel as a precursor and a diethylamine (DEA) template. Detailed synthesis procedures are described in the Experimental Section. As shown in Figure 1, the as-synthesized M-DNL-6 sample displayed rhombic dodecahedral morphology with a particle size in the range of 2–5 μm. Powder XRD (PXRD) patterns (Figure 2) of M-DNL-6 (both as-synthesized and calcined) confirmed the high purity of the RHO structure without any extra phases.[28] The porosity of calcined M-DNL-6 was evaluated by conducting N_2 adsorption experiments at 77 K, and M-DNL-6 exhibited a typical Type I isotherm (Figure 3). The estimated Langmuir surface area was 1096 $m^2 g^{-1}$, and the micropore volume was 0.38 $cm^3 g^{-1}$.

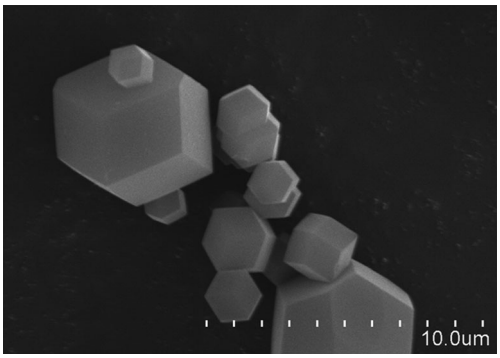

Figure 1. SEM image of the as-synthesized M-DNL-6.

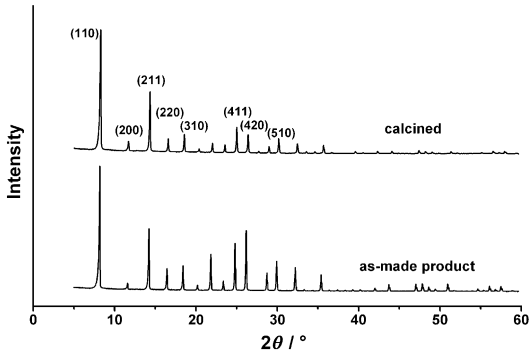

Figure 2. XRD patterns of as-synthesized M-DNL-6 and its calcined form.

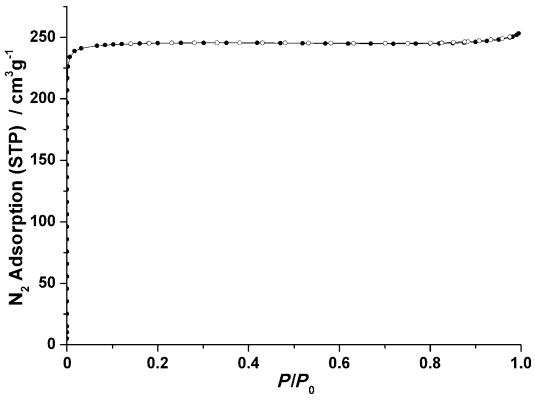

Figure 3. N_2 adsorption (●) and desorption (○) isotherms (77 K) of calcined M-DNL-6.

The major difference between M-DNL-6 (detailed herein) and other DNL-6 materials (synthesized by our previously reported methods) is the Si content of the final product (see Table 1). The amount of Si in M-DNL-6 [Si/(Si+Al+P) = 0.182 mol] is much larger than that of the DNL-6 synthesized by using hydrothermal methods in the presence of cetyltrimethylammonium bromide (CTAB, 0.135 molar ratio; designated as L-DNL-6).[29] Until now, a DNL-6 containing a higher Si content (0.205 molar ratio, designated as H-DNL-6) could only be achieved by using an aminothermal method, which was recently reported by our group.[30] By comparing the initial gel molar ratios to the final product compositions from each method, it was observed that the Si content of DNL-6 increased with increasing template concentration in the gel. The higher template concentration in the synthetic gel could result

Table 1. Gel and product compositions for the synthesis of the different samples.

Sample	Gel composition DEA/Al/P/Si/H_2O	Product composition Si/Al/P	Si incorp.[a]
L-DNL-6	1.0:1.0:0.8:0.2:50:0.1CTAB	0.135:0.496:0.369	1.35
M-DNL-6	1.2:1.0:1.0:0.3:9.3	0.182:0.490:0.328	1.40
H-DNL-6	4.5:1.2:0.9:0.25:8.4	0.205:0.489:0.306	1.93
SAPO-34	1.0:1.0:0.8:0.2:50	0.110:0.506:0.384	–

[a] Si incorporation = $[Si/(Si+Al+P)]_{product}/[Si/(Si+Al+P)]_{gel}$.

in stronger liquid alkalinity, initiating depolymerization of the Si source and resulting in enhanced incorporation of Si in the framework. This was also demonstrated in our previous research regarding the synthesis of SAPO-34.[32] However, all of the methods mentioned above failed to synthesize DNL-6 with adjustable Si content. Varying the amount of Si or the template concentration in the initial gel for each method resulted in the development of a CHA structure, that is, each of the previously reported methods for the synthesis of DNL-6 is limited to a relatively narrow Si concentration range. Herein, we demonstrate the use of three SAPO-based samples with different Si concentrations (H-DNL-6, M-DNL-6, and L-DNL-6) as adsorbents for CO_2 separation.

Adsorption isotherms

The adsorption isotherms of the samples were measured in Micromeritics ASAP 2020 apparatus at a fixed temperature and different pressures (up to 101 kPa). The CO_2 and CH_4 adsorption results on different adsorbents at 298 K are shown in Figure 4 and Table 2. All of the samples indicated that they could adsorb much more CO_2 than CH_4, which was associated with the synergic effects of the small-pore apertures of the adsorbents and the strong quadrupolar interactions of CO_2 with the adsorption sites. The CO_2 uptake of M-DNL-6 reached 4.65 mmol g^{-1} at 298 K and 101 kPa, which was slightly higher than that of NaA (4.48 mmol g^{-1}) and H-DNL-6 (4.30 mmol g^{-1}); however, it was remarkably larger than the adsorption capabilities of L-DNL-6 and SAPO-34, which exhibited uptakes of 3.21 and 3.60 mmol g^{-1}, respectively. The adsorption capacities for CH_4 on the different SAPO-based molecular sieves were similar (0.38–0.46 mmol g^{-1}), but lower than that on NaA

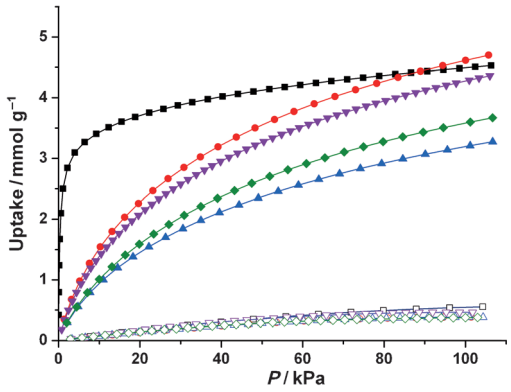

Figure 4. Gas adsorption isotherms of CO_2 (solid) and CH_4 (hollow) on M-DNL-6 (●/○), L-DNL-6 (▶/▷), H-DNL-6 (◀/◁), NaA (■/□) and SAPO-34 (◆/◇) at 298 K.

(0.55 mmol g^{-1}). The behavior of the NaA zeolite towards CH_4 adsorption could be attributed to its larger aperture size.

The highest equilibrium adsorption ratio (α) of CO_2/CH_4 among all of the samples was observed on M-DNL-6 ($\alpha = 12.2$ at 101 kPa). The M-DNL-6 sample demonstrated superior selectivity compared to the other SAPO-based samples. This was clearly evident when the CO_2/CH_4 adsorption ratios were compared at lower pressures (see Table 2), which was useful when the amount of CO_2 to be removed was small. The selectivity obtained on the NaA zeolite in the low-pressure region was much larger ($\alpha = 41.4$ at 10 kPa), which was consistent with the initial slope that was observed in the CO_2 isotherm for the NaA zeolite (Figure 4). This indicated a strong interaction between the large quadrupole moment of CO_2 and the electrostatic field of the NaA zeolite, which was induced by the presence of Na^+ cations.[13,33] In a previous study, extraframework Na^+ ions of the RHO-zeolitic MOF were demonstrated to play a key role in the uptake of CO_2 at lower pressures, whereas the adsorption kinetics largely decreased with increasing pressures.[34] However, the captured CO_2 molecules had a strong affinity and were generally difficult to release under mild conditions; therefore more energy was required to desorb the CO_2 molecules.

For SAPO-type molecular sieves, Si can be incorporated into the framework through a SM2/SM3 substitution mechanism to generate bridging hydroxyl groups (Si–OH–Al).[35,36] Figure 5 illustrates the ^{29}Si magic angle spinning (MAS) NMR spectra for the three DNL-6 samples. Only one intense resonance peak ascribed to the Si(4Al) environment (SM2 substitution) was observed at −92.1 and −91.7 ppm in the spectra for L-DNL-6 and M-DNL-6, respectively. Considering the high Si content in M-DNL-6, this was thought to be unusual and suggested the existence of Si-Al-Si domains in the framework.[37] To our knowledge, such a high concentration of Si(4Al) environments in SAPO-

Table 2. Adsorption data for CO_2 and CH_4 on tested the different samples (298 K).

Sample	CO_2 uptake[a] [mmol g^{-1}]	CH_4 uptake[a] [mmol g^{-1}]	α [n_{CO_2}/n_{CH_4}]	CO_2 uptake[b] [mmol g^{-1}]	CH_4 uptake[b] [mmol g^{-1}]	α [n_{CO_2}/n_{CH_4}]
M-DNL-6	1.52	0.069	22.0	4.65	0.38	12.2
L-DNL-6	0.94	0.070	13.4	3.21	0.38	9.2
H-DNL-6	1.42	0.088	16.1	4.30	0.46	9.3
SAPO-34	1.01	0.075	13.5	3.60	0.37	9.7
NaA	3.48	0.084	41.4	4.48	0.55	8.2

[a] Equilibrium pressure 10 kPa. [b] Equilibrium pressure 101 kPa.

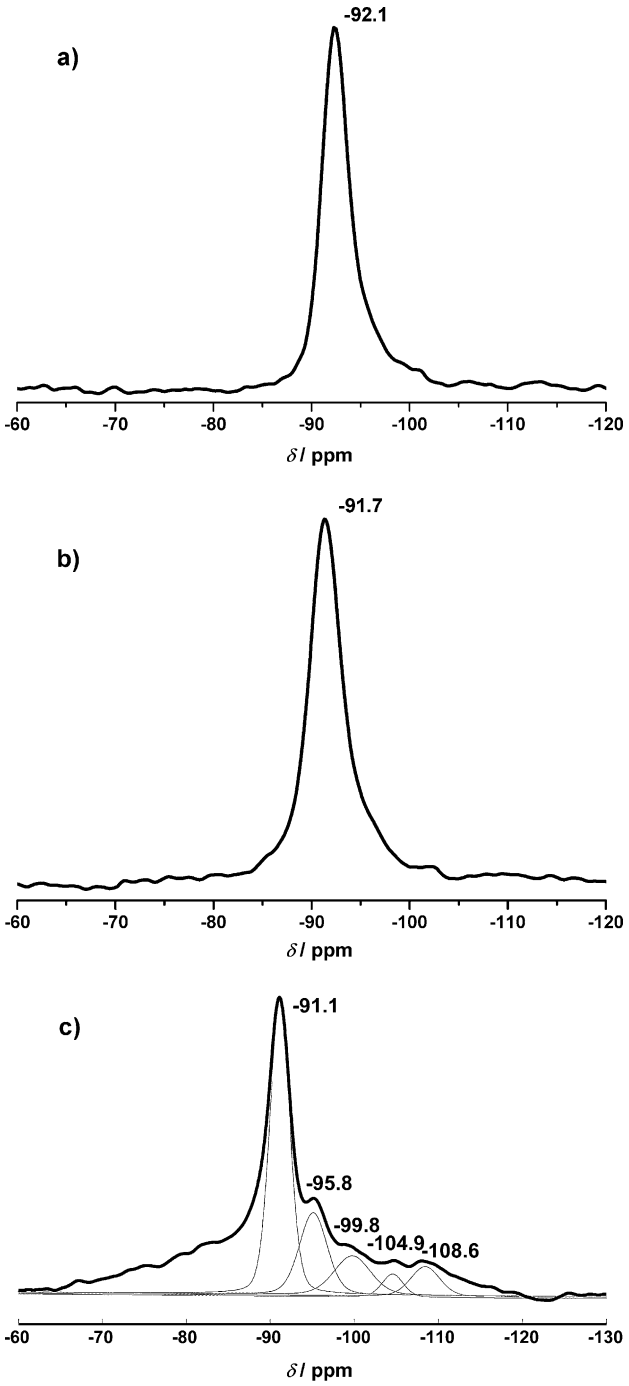

Figure 5. ^{29}Si MAS NMR spectra of as-synthesized a) L-DNL-6, b) M-DNL-6, and c) H-DNL-6.

based molecular sieves has never been reported before. The ^{29}Si MAS NMR spectrum of H-DNL-6 (Figure 5c) revealed complex Si environments; the signals at −95.8, −99.8, −104.9, and −108.6 ppm corresponded to Si(3Al), Si(2Al), Si(1Al), and Si-islands, respectively.[31] The deconvoluted result demonstrated that the concentration of Si(4Al) species in H-DNL-6 occupied 54% of all Si atoms (Table S1). The concentration of Brønsted acid sites in SAPO-based molecular sieves was generally proportional to the Si content when only SM2 substitution occurred, that is, the Brønsted acid sites per Si atom equaled 1. With the appearance of other Si environments in the framework, the Brønsted acid sites per Si atom became less than 1. The maximum Si fraction in the DNL-6 framework, where all the Si atoms contributed to the generation of Brønsted acid sites,[35] was calculated to be 0.178 based on the template number per cage[29] and the RHO topology. The value was close to that of M-DNL-6, indicating that M-DNL-6 possessed the largest concentration of Brønsted acid sites of all four SAPO-based materials. Deroche et al. reported that the Brønsted acid sites in SAPO-based materials were preferential CO_2 adsorption sites, which promoted CO_2 adsorption at the initial stage.[38,39] In addition, Harlick et al. demonstrated that Henry's constant for CO_2 adsorption on H-ZSM-5 zeolites increased with decreasing Si/Al ratios, that is, with an increasing concentration of bridging hydroxyl groups.[40] Our experimental results were in agreement with the above-mentioned conclusions, and M-DNL-6 exhibited a larger CO_2 adsorption capacity and a higher apparent initial slope than L-DNL-6, H-DNL-6, and SAPO-34 (Figure 4). The uptake of CO_2 on M-DNL-6 reached 6.18 mmol g^{-1} at 273 K and 101 kPa (Figure 6).

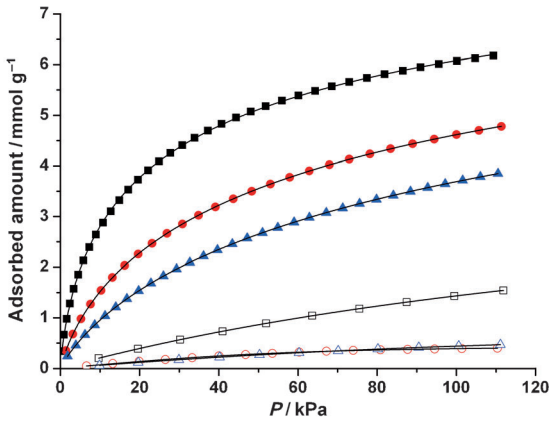

Figure 6. CO_2 (solid) and CH_4 (hollow) adsorption isotherms for M-DNL-6 at 273 (■/□), 298 (●/○), and 313 K (◀/◁); the fittings were based on the Toth equation within correlating error $R^2 = 0.9996$.

The isosteric heat of adsorption data provided useful information about the strength of adsorption and was used to estimate the regeneration ability of the adsorbent. We studied the isosteric heat (Q_{st}) of both CO_2 and CH_4 adsorption on M-DNL-6 from the isotherms collected at 273 K, 298 K, and 313 K. To parameterize the isotherms for single-component gas adsorption, the isotherms of M-DNL-6 were simulated by using the three-parameter Toth model.[25] The Toth equation is a popular model for analyzing gas adsorption data, which is obtained by applying the following equation:

$$q = q_m bp/(1+(bp)^t)^{1/t} \quad (1)$$

Here, q and q_m are the amount adsorbed and the maximum adsorption amount, respectively, p is the equilibrium pressure, and b and t are the equation constants. As described previous-

ly, the parameter t indicates the heterogeneity of the adsorption system. If t equals 1, the Toth isotherm is reduced to the Langmuir adsorption model. If the t value deviates away from 1, the gas–solid adsorption system is deemed to be more heterogeneous. The adsorption uptakes of CO_2 and CH_4 on M-DNL-6 were adequately fitted based on this model. The detailed Toth parameters are detailed in Table S2. The value of isosteric enthalpy with changing adsorption amount was calculated by applying the Clausius–Clapeyron equation, which is described in the Experimental Section.

As shown in Figure 7, the Q_{st} profile of CO_2 adsorption displayed a continuous decline from 39 to 29 kJ mol^{-1} as a function of CO_2 loading. This enthalpy range reflected a relatively

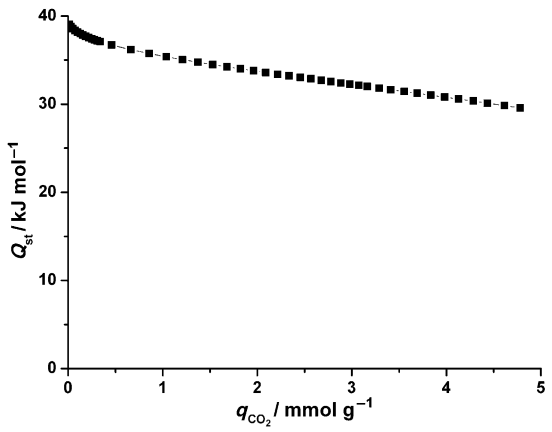

Figure 7. Isosteric heat of adsorption (Q_{st}) as a function of CO_2 loading on M-DNL-6.

strong physical adsorption of CO_2, but still remained below the energy required to form a chemical bond. The high initial Q_{st} value corresponded to the strong interactions of CO_2 with more energetic acidic sites in the framework of M-DNL-6. With an increased CO_2 loading, these sites became saturated and the interaction between adsorbate and adsorbent decreased. We failed to calculate the Q_{st} of CH_4 because the adsorption amount of CH_4 at 313 K was slightly higher than that at 298 K (Figure 6). A possible reason is that CH_4 molecules form small clusters because of intermolecular interactions caused by the Lennard–Jones potential, which was demonstrated by theoretical calculations.[41] Thus, CH_4 cannot freely pass through the pores of the M-DNL-6 adsorbent, and the true adsorption equilibrium is not reached. Palomino et al. observed similar phenomena when they studied CH_4 adsorption on the RHO zeolite.[24]

To estimate the CO_2/N_2 separation efficiency on M-DNL-6, N_2 adsorption isotherms were measured at 273, 298, and 313 K (see Figure S5 in the Supporting Information). The N_2 adsorption uptakes were also fitted to the Toth model, and the measured N_2 capacity in M-DNL-6 was only 0.24 mmol g^{-1} at 298 K and 101 kPa. Therefore, the calculated CO_2/N_2 adsorption ratio under this condition was as high as 19.5.

To further understand the thermodynamic adsorption selectivity on M-DNL-6, the Henry's Law constants for CO_2, CH_4, and N_2 at 298 K were calculated (see the Experimental Section for details).[42] The initial slope for each of the CO_2, CH_4, and N_2 adsorption isotherms are illustrated in the Supporting Information (Figures S6 and S7). From these data, the initial selectivities of CO_2/CH_4 and CO_2/N_2 were evaluated to be as high as 43:1 and 74:1, respectively. These ratios and the high adsorption equilibrium selectivities obtained at atmospheric pressure suggested that M-DNL-6 could be a promising candidate for the removal of CO_2 from natural gas or flue gas.

Breakthrough experiments on M-DNL-6

Breakthrough experiments were performed following a methodology described by Britt et al.;[43] experiments were used to determine the dynamic adsorption selectivity and separation capacity of M-DNL-6 (see the Supporting Information for details). Figure 8 a and b show the breakthrough curves of ternary mixtures of CO_2/CH_4/He (20:15:65 *v/v/v*) and CO_2/N_2/He (20:15:65 *v/v/v*) passing through 0.35 g of pretreated M-DNL-6 powder with a flow rate of 15 mL min^{-1} at 298 K (He acts as the carrier gas). Both CH_4 and N_2 experienced breakthrough quickly as the initial gas mixture was passing through M-DNL-6, but CO_2 was retained in the pores until the adsorbent was saturated. This implied that CH_4 and N_2 could penetrate the packed column with less hindrance. The N_2 effluent was demonstrated to show a shorter retention time than CH_4, in good agreement with the above result that the CO_2/N_2 ad-

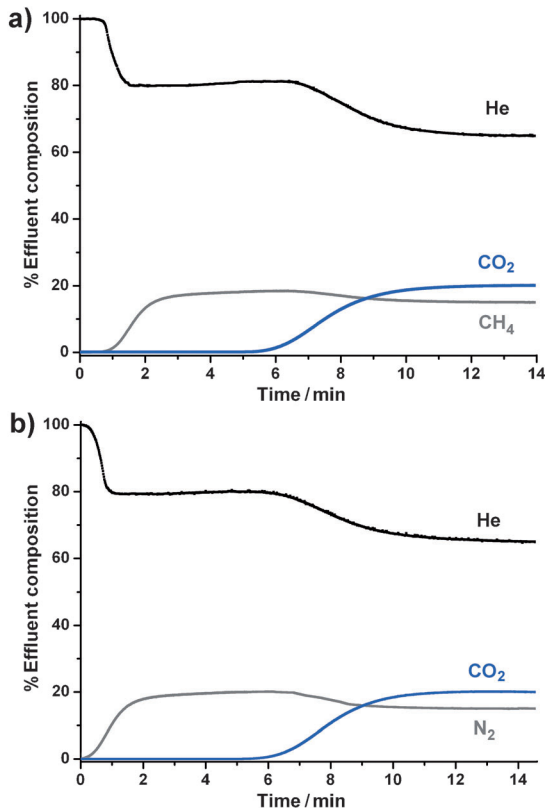

Figure 8. Breakthrough curves of ternary gas mixtures containing a) CO_2/CH_4/He (20:15:65 *v/v/v*) and b) CO_2/N_2/He (20:15:65 *v/v/v*) for the complete retention of CO_2.

sorption equilibrium selectivity was larger than that of CO_2/CH_4. Based on the breakthrough curves of the CO_2/CH_4/He mixture, the dynamic separation capacities of CO_2 and CH_4 on M-DNL-6 were calculated to be 8.0 and 0.29 wt%, respectively. A dynamic capacity ratio of 11 was obtained for CO_2/CH_4, which was close to the thermodynamic selectivity, as presented in Table 2. Based on the CO_2 adsorption capacity and comparison to previous literature reports, M-DNL-6 is one of the most effective adsorbents that has been studied.[43]

Facile regeneration is essential for the adsorbents to be used in the PSA processes, and must require less energy to release the captured CO_2. Consequently, the regeneration capability of M-DNL-6 was examined by using breakthrough experiments. The activated adsorbent was exposed to a binary mixture of gases comprising CO_2/CH_4 (20:80 *v/v*) with a flow rate of 10 mL min^{-1} at 298 K, until the absorbent was saturated with CO_2. Then, the saturated sample was purged with a flow of 20 mL min^{-1} CH_4 for 30 min at the same temperature. Successive operation procedures were repeated for six cycles. To reduce the switching time for the adsorbent regeneration, the M-DNL-6 sample saturated with CO_2 was scrubbed for only 10 min by increasing the regeneration temperature to 333 K. Three cycling breakthrough experiments for the CO_2/N_2 separation were also performed on M-DNL-6 with identical conditions to that of CO_2/CH_4 regeneration. As shown in Figure 9, these cycling tests revealed that M-DNL-6 regained almost 95% of its original CO_2 adsorption capacity under very mild regeneration conditions. Therefore, M-DNL-6 can be proposed as a feasible adsorbent with a large dynamic separation capacity of CO_2 and facile regeneration.

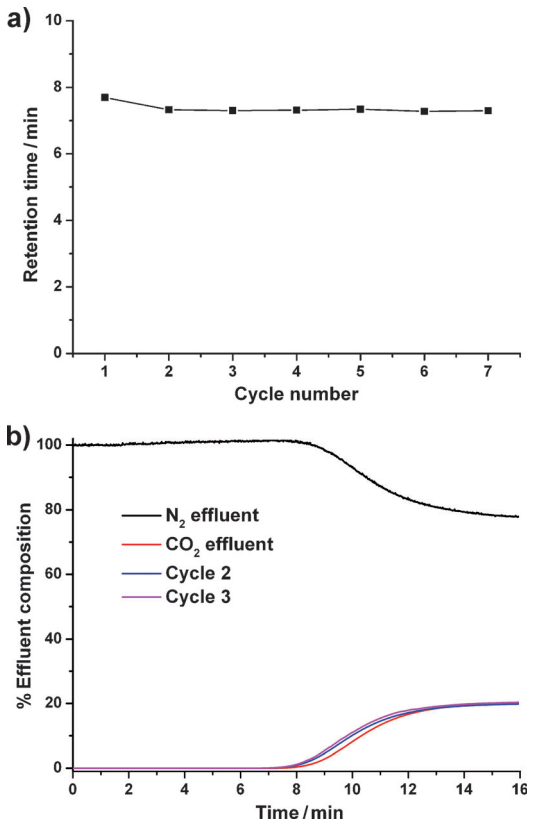

Figure 9. Cycling breakthrough experiments for binary gas separations. a) CO_2 retention time for cycling CO_2/CH_4 separations. Cycle 1: the first breakthrough; cycles 2–6: repeated breakthroughs after the adsorbent had regenerated with CH_4 purge at 298 K for 30 min; cycle 7: adsorbent regenerated with CH_4 purge at 333 K for 10 min. b) Breakthrough cycles for CO_2/N_2 separations with CO_2 and N_2 effluent from the fully regenerated M-DNL-6 and CO_2 effluent obtained from repeated cycles after a N_2 purge at 298 K for 30 min.

Conclusions

We have developed a new method to synthesize a DNL-6 that utilizes SAPO dry gel as the starting material. The product contains a high concentration of Si(4Al) environments [Si/(Si+Al+P) = 0.182 mol], which is the highest value reported for SAPO-based molecular sieves. The large CO_2 adsorption capacity and high selectivity of CO_2/CH_4 and CO_2/N_2 observed on M-DNL-6 can be ascribed to a synergy of the suitable pore aperture and the high concentration of Brønsted acid sites in the material. Breakthrough experiments confirm that M-DNL-6 is selective for the adsorption of CO_2 and requires very mild conditions for regeneration. These characteristics render M-DNL-6 a promising candidate for the selective removal of CO_2 from natural gas or flue gas. Furthermore, M-DNL-6 could be utilized as a promising membrane; the gas separation ability of microporous SAPO-based molecular sieves is greatly increased when they are synthesized as membranes.[44,45]

Experimental Section

Sample synthesis

Typical synthesis of M-DNL-6: an SAPO gel with a molar composition $Al_2O_3/P_2O_5/SiO_2/H_2O$ = 1:1:0.6:50 was prepared by mixing pseudo-boehmite (70.5 wt%), water, phosphoric acid (85 wt%), and silica sol (27.5 wt%) in sequence. The mixture was stirred for 2 h and further milled for 15 min to obtain a homogeneous gel. The dry SAPO gel was obtained by using a spray-drying process. The resulting SAPO material (20 g) was ground into a powder and added to a solution that consisted of DEA (13 g) and water (24 g). The final mixture was transferred into a stainless steel autoclave, sealed, and heated to 468 K under rotation for 9 h. The molar ratio of the gel components were DEA/Al/P/Si/H_2O = 1.2:1:1:0.3:9.3. The as-synthesized products were recovered through filtration, washed with deionized water, and dried at 373 K overnight. The products were then calcined at 873 K for 3 h to remove any organic species for further characterizations.

Detailed synthesis procedures of SAPO-34, L-DNL-6, and H-DNL-6 and characterizations (XRD patterns and SEM images) of these samples are presented in the Supporting Information. These samples were synthesized according to our previously published works.[29–31] The NaA zeolite was purchased as a commercial sample with the molar ratio Na/Si/Al = 1:1:1.

Characterization

PXRD patterns were recorded on a PANalytical X'Pert PRO X-ray diffractometer with CuK_α radiation (λ = 0.15418 nm) operating at 40 kV and 40 mA. Chemical composition of the solid samples was

determined by using a Philips Magix-601 X-ray fluorescence (XRF) spectrometer. SEM imaging was performed on a KYKY-AMRAY-1000B electron microscope at 20 kV. Permanent porosity of the calcined sample was determined by using N_2 adsorption at 77 K on a Micromeritics ASAP 2020 system. Before analysis, the sample was preheated to 623 K under vacuum for 10 h. The total surface area was calculated based on the Langmuir adsorption model. The micropore volume and surface area were evaluated by using the t-plot method. Solid-state ^{29}Si MAS NMR spectroscopy was performed on a Varian Infinityplus-400 spectrometer equipped with a 5 mm MAS probe with a spinning rate of 6 kHz. The spectra were recorded by using high-power proton decoupling; 2000–6000 scans were accumulated with a $\pi/4$ pulse width of 2 μs and a 10 s recycle delay.

Adsorption experiments and calculations

Adsorption isotherms of CO_2, CH_4, and N_2 were measured by using a Micromeritics ASAP 2020 apparatus at 273, 298, and 313 K and pressures up to 101 kPa. The adsorption temperature was controlled by using a Dewar bottle with a circulating jacket connected to a thermostatic bath utilizing water as the coolant. Before analysis, all samples were degassed under a vacuum at 623 K for 10 h. The free space in the tube was determined by using He gas.

On the basis of the collected CO_2, CH_4, and N_2 adsorption isotherms at different temperatures, the enthalpy values (Q_{st}) of CO_2 adsorption in calcined M-DNL-6 were calculated by applying the Clausius-Clapeyron equation:

$$Q_{st} = RT^2\left[\frac{\partial(\ln P)}{\partial T}\right]_{Qi} = R\left[-\frac{\partial(\ln P)}{\partial(1/T)}\right]_{Qi} \quad (2)$$

Here, Q_{st} is the adsorption heat, R is the gas constant, T is temperature, and P is pressure.

Henry's law for selectivity of a single gas component adsorption, i over j, was calculated based on the following equation:

$$S_{i,\,j} = K_i/K_j \quad (3)$$

Here, K_i and K_j are the Henry's law constants for the adsorption components; i and j. K_i and K_j were obtained from the initial slopes of the CO_2, CH_4, and N_2 isotherms.

Breakthrough experiments

The breakthrough experiment setup is shown in Figure S1. The calcined M-DNL-6 powder (0.35 g) was packed between cotton plugs in a quartz sample tube with an internal diameter of 0.46 cm (with a bed height of approximately 2.5 cm). The packed column was initially purged with He (at a flow rate of 15 mL min^{-1}) and heated to 623 K for activation. The He gas remained flowing through the sample tube until the gas flow was changed to the gas mixtures that were used for separation testing. The breakthrough temperature was controlled by using a circulating water thermostatic bath, which was kept at 298 K. Ternary gas mixtures of CO_2/CH_4/He or CO_2/N_2/He with a 20:15:65 (*v/v/v*) ratio were allowed to pass through the sample at a flow rate of 15 mL min^{-1} until all components reached their equilibrium concentration. The effluent gas from the packed column was monitored by using a mass spectrometer. The breakthrough time was defined to be 10% of the feed concentration of each gas. The retention time for detected gases was calculated by subtracting the blank breakthrough time, using the quartz sample tube packed with only cotton plugs, from the observed breakthrough time.

Cycling breakthrough experiments were performed after the activated sample was initially purged with pure CH_4 or N_2 gas flow until no other gases could be detected in the effluent. The sample was then exposed to binary gas mixtures of CO_2/CH_4 or CO_2/N_2 (20:80 *v/v*) with a 10 mL min^{-1} flow rate to detect the first CO_2 breakthrough. Subsequently, the CO_2-saturated sample was purged with 20 mL min^{-1} of CH_4 or N_2 for 30 min at 298 K for cycling breakthrough tests.

Acknowledgements

We are grateful for the financial support from the National Natural Science Foundation of China (NSFC 21101150).

Keywords: adsorption · aluminosilicates · carbon dioxide separation · regeneration · zeolites

[1] J. R. Li, R. J. Kuppler, H. C. Zhou, *Chem. Soc. Rev.* **2009**, *38*, 1477–1504.
[2] A. Corma, F. Rey, J. Rius, M. J. Sabater, S. Valencia, *Nature* **2004**, *431*, 287–290.
[3] B. L. Chen, S. C. Xiang, G. D. Qian, *Acc. Chem. Res.* **2010**, *43*, 1115–1124.
[4] R. Matsuda, R. Kitaura, S. Kitagawa, Y. Kubota, R. V. Belosludov, T. C. Kobayashi, H. Sakamoto, T. Chiba, M. Takata, Y. Kawazoe, Y. Mita, *Nature* **2005**, *436*, 238–241.
[5] J. Caro, M. Noack, *Microporous Mesoporous Mater.* **2008**, *115*, 215–233.
[6] B. L. Chen, C. D. Liang, J. Yang, D. S. Contreras, Y. L. Clancy, E. B. Lobkovsky, O. M. Yaghi, S. Dai, *Angew. Chem.* **2006**, *118*, 1418–1421; *Angew. Chem. Int. Ed.* **2006**, *45*, 1390–1393.
[7] B. Wang, A. P. Côté, H. Furukawa, M. O'Keeffe, O. M. Yaghi, *Nature* **2008**, *453*, 207–211.
[8] K. Sumida, D. L. Rogow, J. A. Mason, T. M. McDonald, E. D. Bloch, Z. R. Herm, T. H. Bae, J. R. Long, *Chem. Rev.* **2012**, *112*, 724–781.
[9] S. Li, J. G. Martinek, J. L. Falconer, R. D. Noble, T. Q. Gardner, *Ind. Eng. Chem. Res.* **2005**, *44*, 3220–3228.
[10] M. Tagliabue, D. Farrusseng, S. Valencia, S. Aguado, U. Ravon, C. Rizzo, A. Corma, C. Mirodatos, *Chem. Eng. J.* **2009**, *155*, 553–566.
[11] K. S. Walton, M. B. Abney, M. D. LeVan, *Microporous Mesoporous Mater.* **2006**, *91*, 78–84.
[12] S. Choi, J. H. Drese, C. W. Jones, *ChemSusChem* **2009**, *2*, 796–854.
[13] M. Palomino, A. Corma, F. Rey, S. Valencia, *Langmuir* **2010**, *26*, 1910–1917.
[14] S. R. Venna, M. A. Carreon, *J. Phys. Chem. B* **2008**, *112*, 16261–16265.
[15] D. Q. Vu, W. J. Koros, S. J. Miller, *Ind. Eng. Chem. Res.* **2002**, *41*, 367–380.
[16] Y. S. Bae, R. Q. Snurr, *Angew. Chem.* **2011**, *123*, 11790–11801; *Angew. Chem. Int. Ed.* **2011**, *50*, 11586–11596.
[17] J. An, S. J. Geib, N. L. Rosi, *J. Am. Chem. Soc.* **2010**, *132*, 38–39.
[18] K. Morishige, *J. Phys. Chem. C* **2011**, *115*, 9713–9718.
[19] D. W. Breck, *Zeolite Molecular Sieves*, Wiley, New York, **1974**.
[20] D. Baowan, *J. Math. Chem.* **2012**, *50*, 300–309.
[21] O. Cheung, Q. Liu, Z. Bacsik, N. Hedin, *Microporous Mesoporous Mater.* **2012**, *156*, 90–96.
[22] S. Himeno, T. Tomita, K. Suzuki, S. Yoshida, *Microporous Mesoporous Mater.* **2007**, *98*, 62–69.
[23] X. Si, C. Jiao, F. Li, J. Zhang, S. Wang, S. Liu, Z. Li, L. Sun, F. Xu, Z. Gabelica, C. Schick, *Energy Environ. Sci.* **2011**, *4*, 4522–4527.
[24] M. Palomino, A. Corma, J. L. Jordá, F. Rey, S. Valencia, *Chem. Commun.* **2012**, *48*, 215–217.
[25] Q. Liu, C. N. O. Cheung, A. E. Garcia-Bennett, N. Hedin, *ChemSusChem* **2011**, *4*, 91–97.
[26] F. Akhtar, Q. Liu, N. Hedin, L. Bergström, *Energy Environ. Sci.* **2012**, *5*, 7664–7673.
[27] M. M. Lozinska, E. Mangano, J. P. S. Mowat, A. M. Shepherd, R. F. Howe, S. P. Thompson, J. E. Parker, S. Brandani, P. A. Wright, *J. Am. Chem. Soc.* **2012**, *134*, 17628–17642.

[28] P. Tian, X. Su, Y. Wang, Q. Xia, Y. Zhang, D. Fan, S. Meng, Z. Liu, *Chem. Mater.* **2011**, *23*, 1406 – 1413.
[29] X. Su, P. Tian, J. Li, Y. Zhang, S. Meng, Y. He, D. Fan, Z. Liu, *Microporous Mesoporous Mater.* **2011**, *144*, 113 – 119.
[30] D. Fan, P. Tian, S. Xu, Q. Xia, X. Su, L. Zhang, Y. Zhang, Y. He, Z. Liu, *J. Mater. Chem.* **2012**, *22*, 6568 – 6574.
[31] G. Liu, P. Tian, J. Li, D. Zhang, F. Zhou, Z. Liu, *Microporous Mesoporous Mater.* **2008**, *111*, 143 – 149.
[32] G. Liu, P. Tian, Y. Zhang, J. Li, L. Xu, S. Meng, Z. Liu, *Microporous Mesoporous Mater.* **2008**, *114*, 416 – 423.
[33] P. J. E. Harlick, F. H. Tezel, *Microporous Mesoporous Mater.* **2004**, *76*, 71 – 79.
[34] R. Babarao, J. Jiang, *Energy Environ. Sci.* **2009**, *2*, 1088 – 1093.
[35] R. Vomscheid, M. Briend, M. J. Peltre, P. P. Man, D. Barthomeuf, *J. Phys. Chem.* **1994**, *98*, 9614 – 9618.
[36] A. M. Prakash, S. Unnikrishnan, *J. Chem. Soc. Faraday Trans.* **1994**, *90*, 2291 – 2296.
[37] D. Barthomeuf, *J. Phys. Chem.* **1993**, *97*, 10092 – 10096.
[38] I. Deroche, L. Gaberova, G. Maurin, M. Castro, P. A. Wright, P. L. Llewellyn, *J. Phys. Chem. C* **2008**, *112*, 5048 – 5056.
[39] I. Deroche, L. Gaberova, G. Maurin, P. Llewellyn, M. Castro, P. Wright, *Adsorption* **2008**, *14*, 207 – 213.
[40] P. J. E. Harlick, F. H. Tezel, *Sep. Purif. Technol.* **2003**, *33*, 199 – 210.
[41] H. Takeuchi, *Comput. Theor. Chem.* **2012**, *986*, 48 – 56.
[42] L. Czepirski, J. Jagiełło, *Chem. Eng. Sci.* **1989**, *44*, 797 – 801.
[43] D. Britt, H. Furukawa, B. Wang, T. G. Glover, O. M. Yaghi, *Proc. Natl. Acad. Sci. USA* **2009**, *106*, 20637 – 20640.
[44] M. A. Carreon, S. Li, J. L. Falconer, R. D. Noble, *J. Am. Chem. Soc.* **2008**, *130*, 5412 – 5413.
[45] M. A. Carreon, S. Li, J. L. Falconer, R. D. Noble, *Adv. Mater.* **2008**, *20*, 729 – 732.

Received: November 29, 2012
Published online on April 18, 2013